RAPID WITH DOUBLE-TURN COIL OSH-MPT ARRAY FOR DAMAGE DETECTION IN COMPOSITE PLATE

Zenghua Liu[1], Xuwen Zhong[1], Honglei Chen[1], Cunfu He[1], and Bin Wu[1]

[1]College of Mechanical Engineering and Applied Electronics Technology, Beijing University of Technology, Beijing 100124, China
liuzenghua@bjut.edu.cn, zhongxuwen@emails.bjut.edu.cn, hl.chen87@foxmail.com, hecunfu@bjut.edu.cn, wubin@bjut.edu.cn
web page: http://cekong.bjut.edu.cn/

Keywords: Composite plate, RAPID, Shear-horizontal waves, Damage imaging, Magnetostrictive patch transducer

ABSTRACT

Imaging detection of composite plates is presented based on reconstruction algorithm for the probabilistic inspection of damage (RAPID) and double-turn coil omnidirectional shear-horizontal wave magnetostrictive patch transducer (OSH-MPT) array. The lowest shear-horizontal mode (SH_0) can propagate in the composite plate through bonding double-turn coil OSH-MPT. RAPID can realize using the direct wave of SH_0 mode to extract the damage information. It is beneficial to detect composite plate in the case that the velocity of direct waves varies with the propagation direction. A small mass which is circular cylinder is bonded to simulate damage. Imaging results are achieved after using modified methods for eliminating the influence of the uneven probability distribution of the array (UPDA) in RAPID. Threshold is selected based on the receiver operating characteristic (ROC) curve for improving RAPID-based imaging accuracy.

1 INTRODUCTION

Composite plates are increasingly used in aerospace, automobile manufacturing, ship transportation and other fields. The application of non-destructive testing (NDT) technology can meet the requirement to detect the existence of damage, non-uniformity of the specimen and quantitative analysis of damage without destroying pristine structures. Structural health monitoring (SHM) develops on the basis of technological innovation of NDT. However, unlike most NDT methods, transducers are bonded or embedded in the structures to realize on-line detection [1]. Ultrasonic guided waves based SHM has shown significant promise to promptly and efficiently achieve feature analysis and real-time monitoring of plates with finite transducers.

As a new type of electromagnetic acoustic transducer (EMAT), magnetostrictive patch transducer (MPT) has broadened the applied range of EMAT [2]. MPT generally contains the magnetostrictive patch contacting to plates in addition to the magnet and coil. Although MPT loses the EMAT non-contact characteristics, but the signal to noise ratio is effectively improved. Lee et al. [3] developed a kind of MPT which used planar solenoid array coil (PSA) in the aluminium plate to excite the high-energy directivity SH_0 mode. PSA integrated the advantages of meander coil and figure-of-eight coil. Seung et al. [4] proposed an OSH-MPT to generate omnidirectional SH_0 mode in aluminium plates.

Imaging technology provides the basis for damage visualization in order to intuitively and clearly display related information of damage. Hay et al. [5] summarized some ultrasonic tomography methods and compared the application characteristics of different tomography methods. At the same time, the method of RAPID based Lamb waves was proposed. Zhao et al. [6] used a sparse PZT array and detected crack near the rivet hole on the aluminium wing of the aircraft through the correlation analysis based on RAPID. RAPID is one of ultrasonic tomography algorithms that calculate the probability of damage in the imaging area.

In this study, it is proved that combining MPT array with RAPID imaging can be applied to damage detection and have potential for SHM in composite plates. Imaging principle of RAPID is studied in Section 2. In Section 3, RAPID parameters are calculated and simulated damage imaging results are

presented. RAPID imaging threshold based on ROC curve is selected for improving imaging quality. Brief conclusions are given in Section 4.

2 IMAGING PRINCIPLE OF RAPID

Generally, imaging area should be set during the imaging process. RAPID is the imaging method to represent the damage probability estimation of every point in imaging area. A pair of transducer is hard to identify damage accurately and clearly. Therefore, image fusion approaches are used to integrate images formed by transducer pairs. RAPID-based full summation imaging is defined as [6]:

$$P(x,y)=\sum_{i=1}^{N}\sum_{j=1,i\neq j}^{N}P_{ij}(x,y)=\sum_{i=1}^{N}\sum_{j=1,i\neq j}^{N}A_{ij}\frac{\beta+1-R_{ij}(x,y)}{\beta} \tag{1}$$

where $P(x,y)$ is the estimated damage probability value at point (x,y) through RAPID-based full summation method; N are total transducer pairs.

RAPID-based full multiplication imaging is defined as [7]:

$$Q(x,y)=\prod_{i=1}^{N}\prod_{j=1,i\neq j}^{N}Q_{ij}(x,y)=\prod_{i=1}^{N}\prod_{j=1,i\neq j}^{N}\left[A_{ij}\frac{\beta+1-R_{ij}(x,y)}{\beta}+1\right] \tag{2}$$

where $Q(x,y)$ is the estimated damage probability value at point (x,y) through RAPID-based full multiplication method. Every transducer pair ij corresponds to one sensing path, one $P_{ij}(x,y)$ and one $Q_{ij}(x,y)$. Baseline signals which are acquired under undamaged specimen are compared with damage signal. $R_{ij}(x,y)$ is defined as:

$$R_{ij}(x,y)=\begin{cases}RD_{ij}(x,y), & RD_{ij}(x,y)\leq\beta+1\\ \beta+1, & RD_{ij}(x,y)>\beta+1\end{cases} \tag{3}$$

where $RD_{ij}(x,y)$ is defined as:

$$RD_{ij}(x,y)=\frac{\sqrt{(x_i-x)^2+(y_i-y)^2}+\sqrt{(x_j-x)^2+(y_j-y)^2}}{\sqrt{(x_i-x_j)^2+(y_i-y_j)^2}} \tag{4}$$

$RD_{ij}(x,y)$ is related to the coordinate of transmitter (x_i,y_i), receiver (x_j,y_j) and arbitrary point (x,y) at imaging area. It can conclude the $RD_{ij}(x,y)\geq 1$ from Equation (4). The maximum effective detection area of transducer pair ij appears ellipse shape. Parameter β determines the size of ellipse shape. Figure 1 shows the value of $R_{ij}(x,y)$ for transducer pair ij. The blue area is the effective detection area where $R_{ij}(x,y)=RD_{ij}(x,y)$. The gray area is invalid detection area where $R_{ij}(x,y)=\beta+1$. $P(x,y)=0$ and $Q(x,y)=1$ when $R_{ij}(x,y)=\beta+1$. $P(x,y)>0$ and $Q(x,y)>1$ if the effective detection area exists damage.

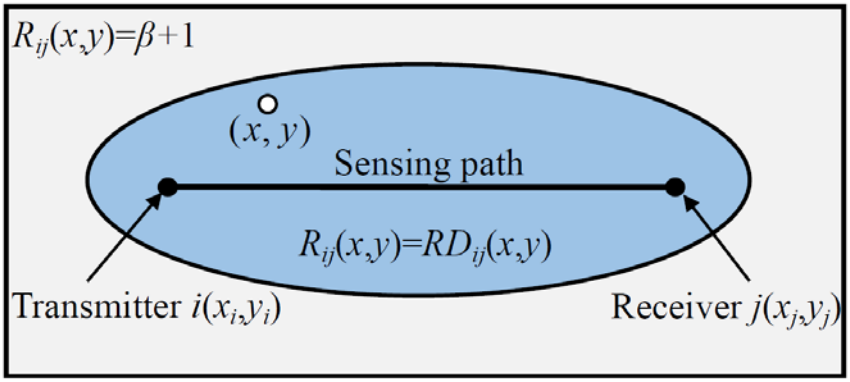

Figure 1: The value of $R_{ij}(x,y)$ for transducer pair ij.

Figure 2 shows the probability value distribution for transducer pair *ij*. Brown ellipse means the maximum probability value while blue ellipse means the minimum probability value. The probability value decreases progressively. If points of imaging area meet the distance from transmitter *i* to the point added by the distance from the point to receiver is identical, these points will locate at the same ellipse. $RD_{ij}(x,y)$ is positive value so that $P_{ij}(x,y)$ and $Q_{ij}(x,y)$ are inversely proportional to $RD_{ij}(x,y)$ through Equations (1) and (2), respectively. The further distance away sensing path of transducer pair *ij*, the smaller probability value is. Therefore, the probability value distribution appears multiple ellipses.

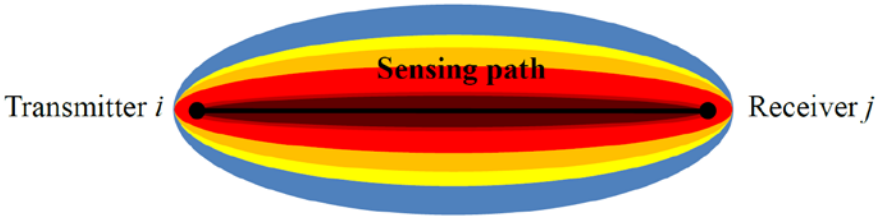

Figure 2: Probability value distribution for transducer pair *ij*.

A_{ij} is the signal difference coefficient (SDC) for measuring the difference between baseline signal and damage signal. A_{ij} is defined as:

$$SDC = 1 - \frac{C_{DB}}{\sigma_D \sigma_B} = \frac{\sum_{t=0}^{t_a} [D(t) - \mu_{D(t)}][B(t) - \mu_{B(t)}]}{\sqrt{\sum_{t=0}^{t_a} [D(t) - \mu_{D(t)}]^2 \sum_{t=0}^{t_a} [B(t) - \mu_{B(t)}]^2}} \tag{5}$$

where $D(t)$ is damage signal; $B(t)$ is baseline signal; $\mu_{D(t)}$ and $\mu_{B(t)}$ are the standard deviation of $D(t)$ and $B(t)$, respectively; σ_D and σ_B are the mean value of $D(t)$ and $B(t)$, respectively; C_{DB} is the covariance of $D(t)$ and $B(t)$. Higher value of SDC means the greater difference in $D(t)$ and $B(t)$.

3 EXPERIMENTS

3.1 Experimental system

Figure 3 shows experimental system for RAPID-based imaging, which includes a PC with control software, a high power ultrasonic measurement system RITEC-RAM-5000, an impedance matching box for transmitter, an oscilloscope DPO4054, a preamplifier, an impedance matching box for receiver, and double-turn coil OSH-MPT array bonded on the sample plate through epoxy glue. The sample plate is a 16-layer quasi-isotropic carbon fiber-reinforced composite plate T300/QY8911 which has 1000mm in length, 1000mm in width and 2.24mm in thickness with $[(0/45/90/-45)_2]_s$ lay-up. The double-turn coil OSH-MPT array has 500mm in diameter and the black circle denotes transducer as illustrated in Figure 3. The blue dotted line is imaging area of 600mm×600mm. The array center locates at (300, 300).

The double-turn coil OSH-MPT is mainly made up of a cylindrical NdFeB magnet, an annular nickel patch and a toroidal coil as shown in Figure 3. The toroidal coil is winded by varnished wire to assemble an annular organic glass patch and the nickel patch. Evenly spaced circular holes are in the organic glass patch for making the toroidal coil. The lift-off distance of cylindrical magnet is achieved through a supporting sleeve. The cylindrical magnet produces a radial static magnetic field which is perpendicular to circumferential dynamic magnetic field provided by the energized toroidal coil. Shear deformation generates in the nickel patch due to the interaction of static magnetic field and dynamic magnetic field based on magnetostrictive phenomena. It has been verified that SH_0 mode can be excited and received in composite plate through bonded double-turn coil OSH-MPT [8].

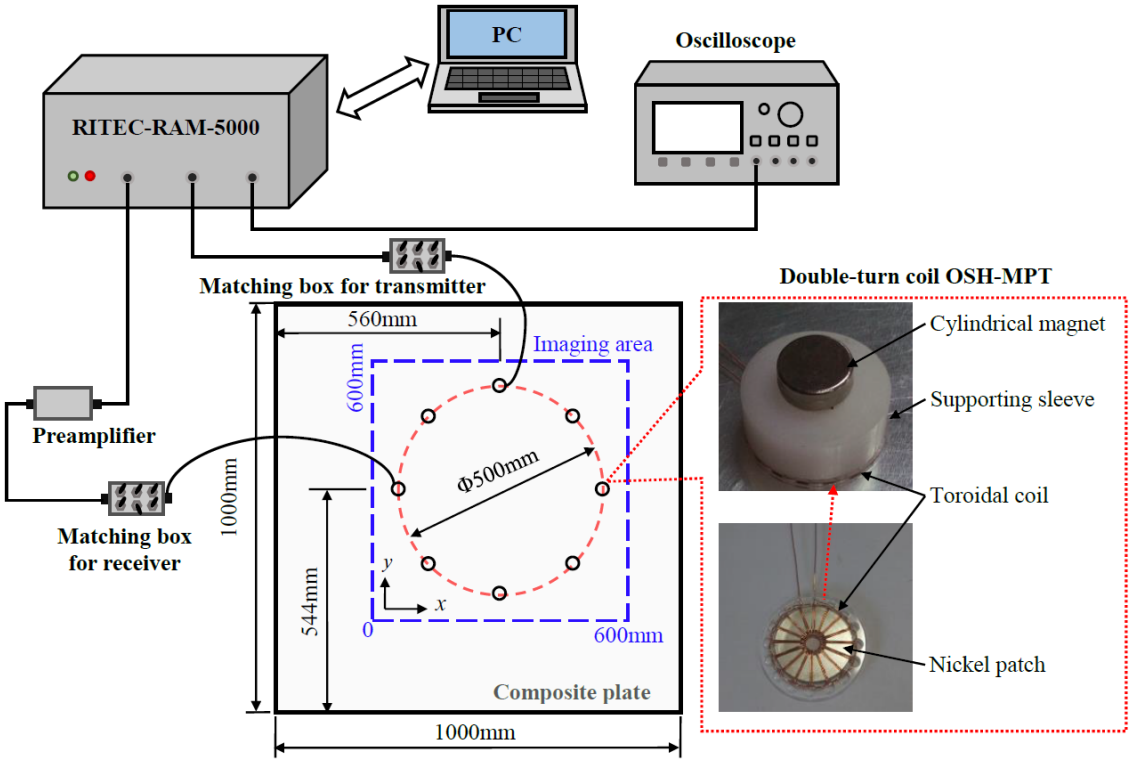

Figure 3: Diagram of experimental system for RAPID-based imaging.

3.2 Calculation of parameter β

According to imaging principle of RAPID, the ellipse boundary of the maximum effective detection area of transducer pair is formed when $RD_{ij}(x,y)=\beta+1$. This paper selects the appropriate β value under the case of experimental transducer array as shown in Figure 3.

Four types of sensing paths are in eight transducers of array as illustrated in Figure 4. Namely, the sensing paths between two transducers which are separated by three transducers, two transducers and one transducer are shown in Figure 4(a), 4(b) and 4(c), respectively. The sensing path between two adjacent transducers is shown in Figure 4(d). For the outer area of the circular array, the fusion number of images is not enough to achieve precise detection results. Thus, when the transducers are arranged to a circular array, the effective detection range of array is limited to the interior area of the array. The elliptical boundary of the maximum effective detection area of transducer pair is tangent to the edge of the circular array with two transducers as the focuses of the ellipse. Based on the elliptical boundary, the four types of sensing paths correspond to four β values that are 0.4, 0.2, 0.08 and 0.02 as shown in Figure 4.

Next, the appropriate β value is optimized. Figure 5 shows the effective detection range of the array when β values are 0.02 and 0.08. As can be seen from Figure 5(a), non-detection zone exists within the effective detection range of the array when β value is 0.02. When the β value is greater than or equal to 0.08, there is no non-detection zone in the detection range. Figure 6 shows probability value distributions formed by sensing paths at different β values. When the β value is greater than or equal to 0.2, the maximum effective detection area of single sensor path covers more than half of the array area so that probability value of detection area appears too large without damage. Because damage imaging result is finally made by fusing imaging results of multiple sensing paths, the original probability value of detection area is too large that easily leads to reduce imaging contrast. By the above analysis, β value of 0.08 is more reasonable, and its rationality will be further proved in the following Subsection 3.4.

According to the circular array of eight double-turn coil OSH-MPTs in the experiment, the β value is determined to be 0.08. The calculation method of β is summarized as follows. Four types of sensing paths of array correspond to four possible β values. The proper β value needs to meet three requirements. Firstly, the effective detection area of all sensor pairs in the array is superimposed to cover the inner

area of the array without non-detection zone. Secondly, the number of imaging result formed by transducer pair is reduced for improving imaging speed after meeting the first requirement. Thirdly, the maximum effective detection area formed by each sensor path is less than half of the area of the array in order to reduce the influence of too large probability value distribution in the array without damage. β=0.08 is suitable for eight circular transducer array at any diameter because the ratio of the distance of each transducer pair is constant when calculating the four β values.

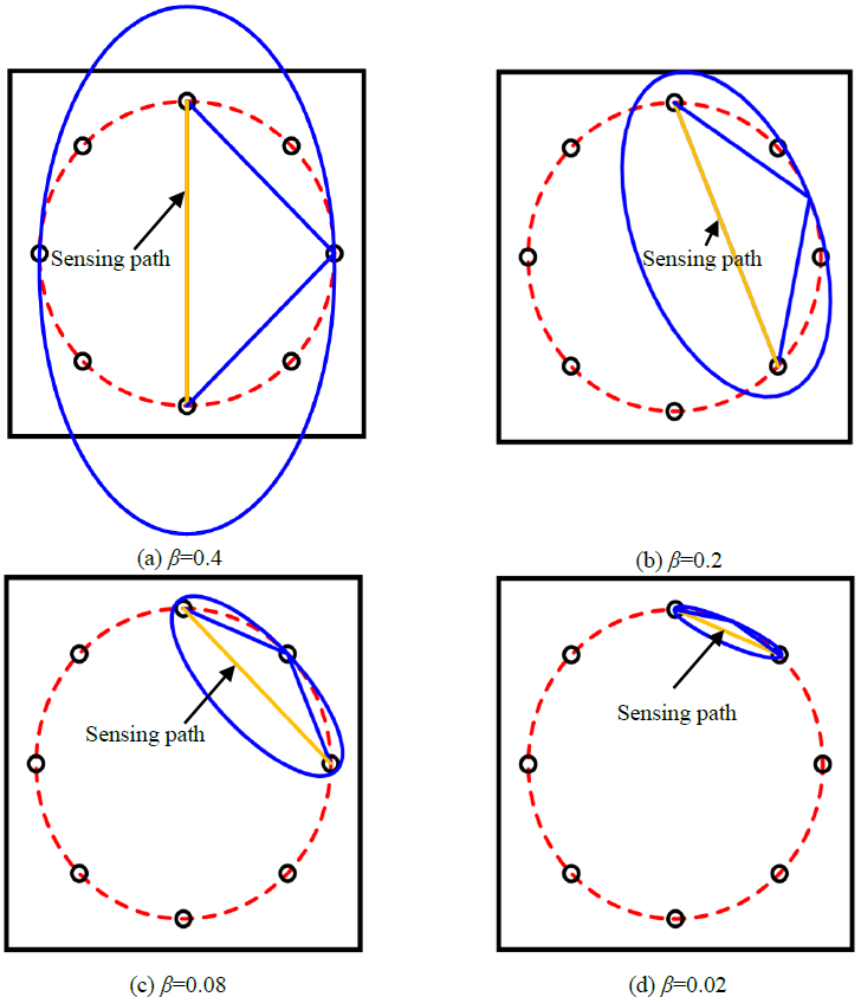

(a) β=0.4 (b) β=0.2

(c) β=0.08 (d) β=0.02

Figure 4: Four types of sensing paths and corresponding β values in eight transducers of array.

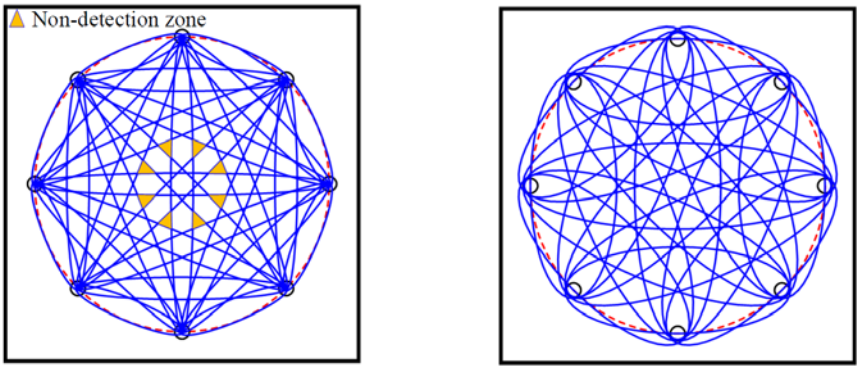

(a) β=0.08 (b) β=0.02

Figure 5: Effective detection range of the array at different β values.

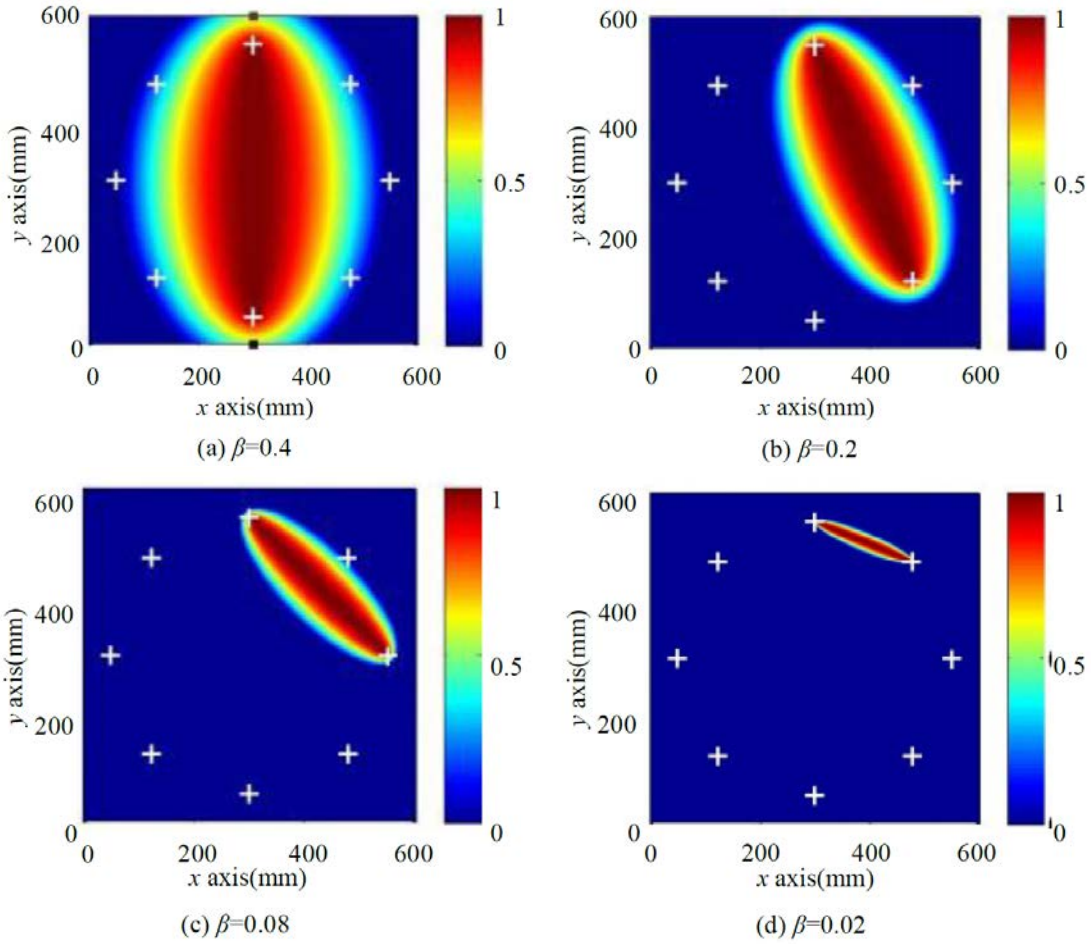

Figure 6: Probability value distributions formed by sensing paths at different β values.

3.3 The UPDA in RAPID

As shown in Figure 2, the probability value distribution of a pair of transducers decreases from the inside to the outside in the RAPID. When multiple images formed by all transducer pair are fused, there is a phenomenon of UPDA in RAPID as shown in Figure 7. The color distribution in the Figure 7 is inconsistent from the center point to the outer boundary. The UPDA is the inherent phenomenon in RAPID, which does not disappear due to different β values or A_{ij}.

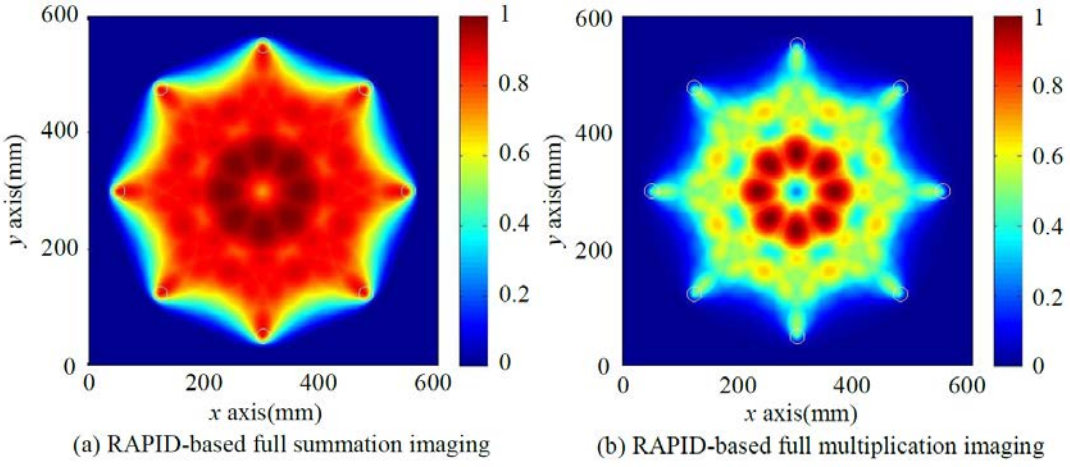

Figure 7: Phenomenon of UPDA in RAPID.

3.4 Damage imaging results

Experimental system and the arrangement of double-turn OSH-MPT array are shown in Figure 3. A boned cylinder with height of 50mm and the bottom diameter of 30mm was used as simulated damage by epoxy resin. And the center coordinates of the bonded cylinder were (339,315). Eight transducers totally formed 56 sensing paths. Each transducer pair collected damage signal and baseline signal to compare for calculating the corresponding A_{ij} value.

3.4.1 Imaging results at different β values

According to the analysis of Subsection 3.2, the four possible β values are 0.4, 0.2, 0.08 and 0.02. Imaging results at different β values are illustrated in Figure 8. When β=0.4 and β=0.2, the dark range with high probability value are large so that imaging contrast ratio is low. The presence of non-detection zone leads to inaccuracy of damage location at β=0.02. β=0.08 can make up for the disadvantages of the above β values and improve the positioning accuracy. The imaging results verify the reasonability of β=0.08.

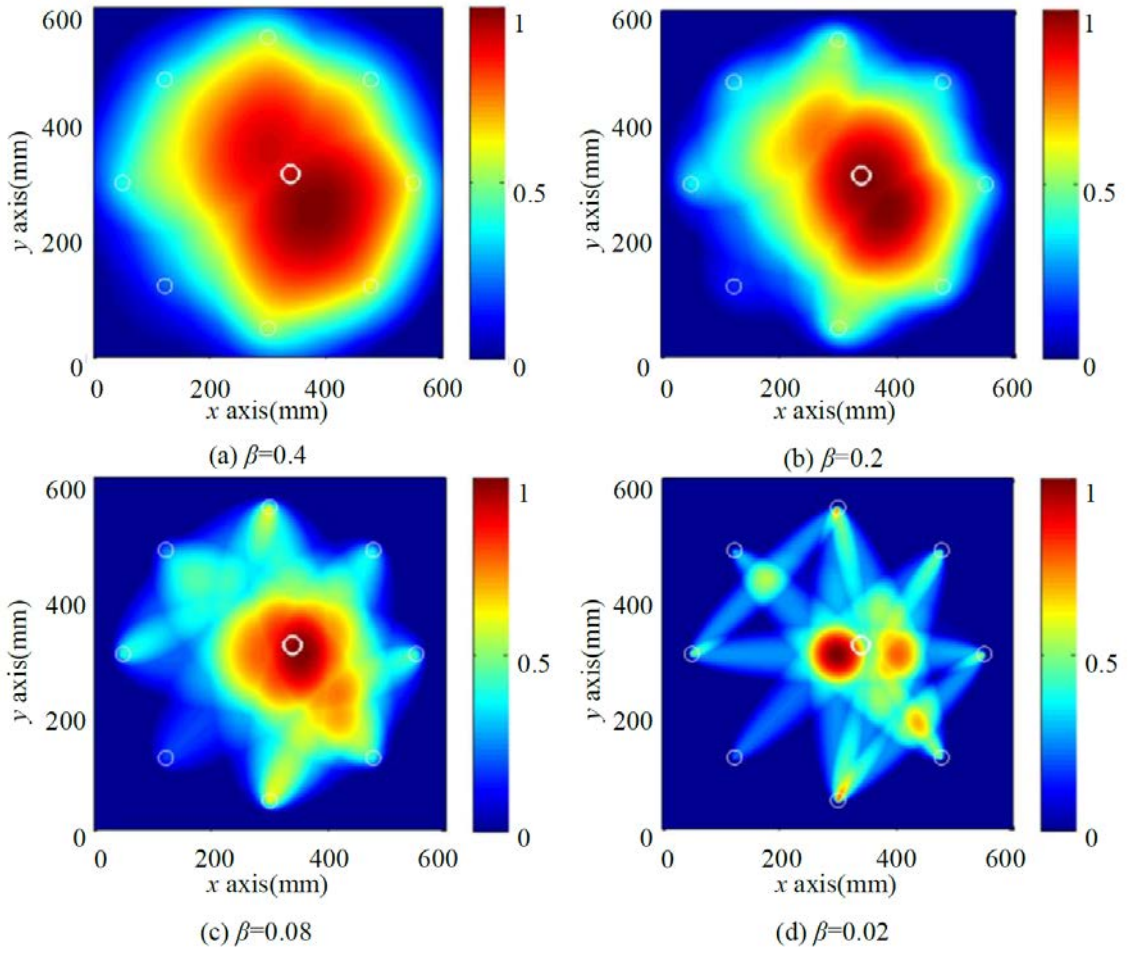

Figure 8: Imaging results at different β values.

3.4.2 Imaging results before and after eliminating the influence of UPDA

In Subsection 3.3, we analyze the inherent UPDA in the RAPID. Since UPDA cannot be eliminated, the influence of UPDA on the imaging is modified through improving the damage contrast. Theoretical A_{ij} is zero in the absence of damage, but actual A_{ij} is not zero because of external interference. In this paper, we set the average value of the maximum and minimum values, A_{avg}, into the imaging formula to produce an image with UPDA. A_{avg} is a definite value and does not change due to the change of sensing paths, and UPDA shown in Figure 7 is the same. Methods are applied to modify the influence of UPDA on RAPID-based full summation imaging and RAPID-based full multiplication imaging. In

the case of damage, an original image with the actual A_{ij} is generated. For the RAPID-based full summation imaging, the image with UPDA is subtracted from the original image. For RAPID-based full multiplication imaging, the original image is divided by the image with UPDA.

Figure 9 presents the RAPID-based full summation imaging results before and after using modified method for the influence of UPDA. Figure 9(a) shows the original image of detecting damage with the influence of UPDA. Figure 10 shows the probability value curves before using modified method for the influence of UPDA, and corresponds to the image of Figure 9(a). Figure 10(a) is the normalized probability value of the *x*-axis coordinate of each imaging point. Figure 10(b) is the normalized probability value of the *y*-axis coordinate of each imaging point. Points with the highest normalized probability value are the *x*-axis coordinate and *y*-axis coordinate of the center of detected damage in Figure 10(a) and Figure 10(b), respectively. Figure 11 shows the probability value curves after using modified method for the influence of UPDA, and corresponds to the image of Figure 9(b). The actual center coordinates of simulated damage are (339,315). From the results presented in Figures 10 and 11, the detected center coordinates of simulated damage are (352,304) before using modified method, whereas (338,312) after using modified method. Figure 12 presents the RAPID-based full multiplication imaging results before and after using modified method for the influence of UPDA. The detected center coordinates of simulated damage are (353,309) before using modified method, whereas (337,312) after using modified method. Therefore, contrast ratio of imaging is higher and imaging accuracy is improved after using modified methods for eliminating the influence of UPDA.

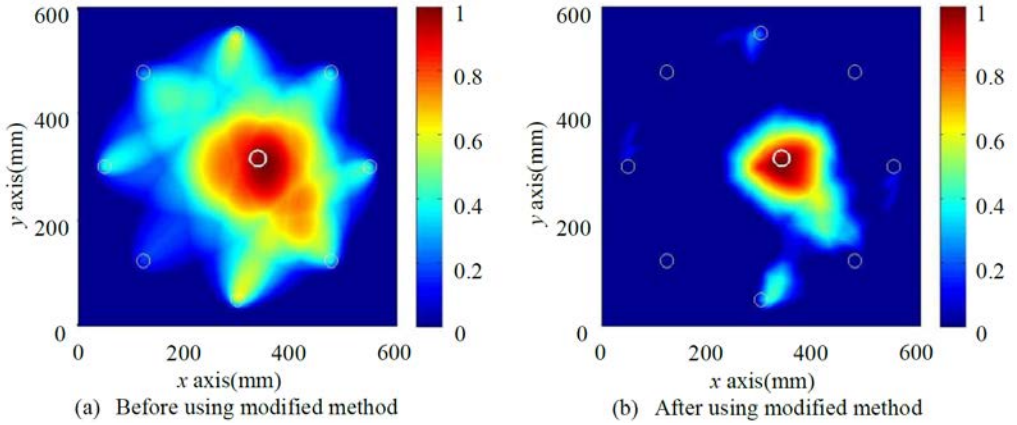

Figure 9: RAPID-based full summation imaging results before and after using modified method for the influence of UPDA.

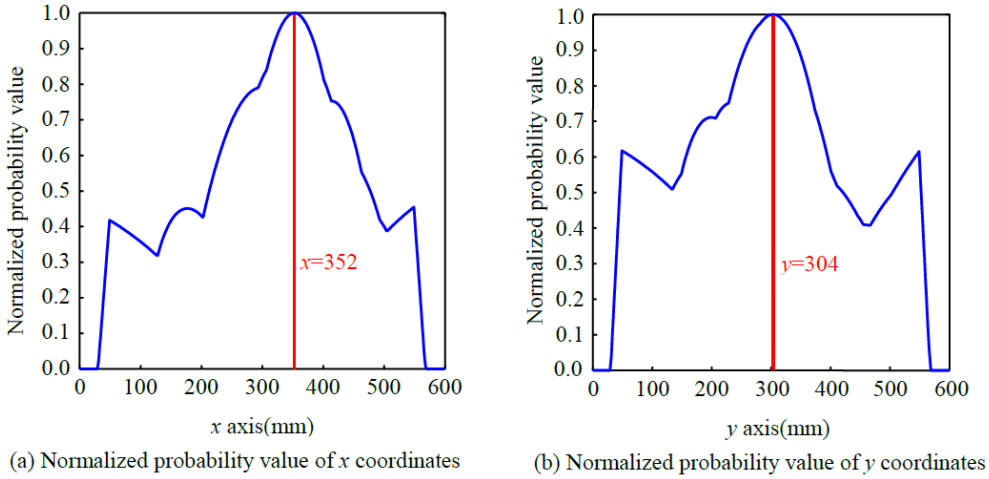

Figure 10: Probability value curves before using modified method for the influence of UPDA.

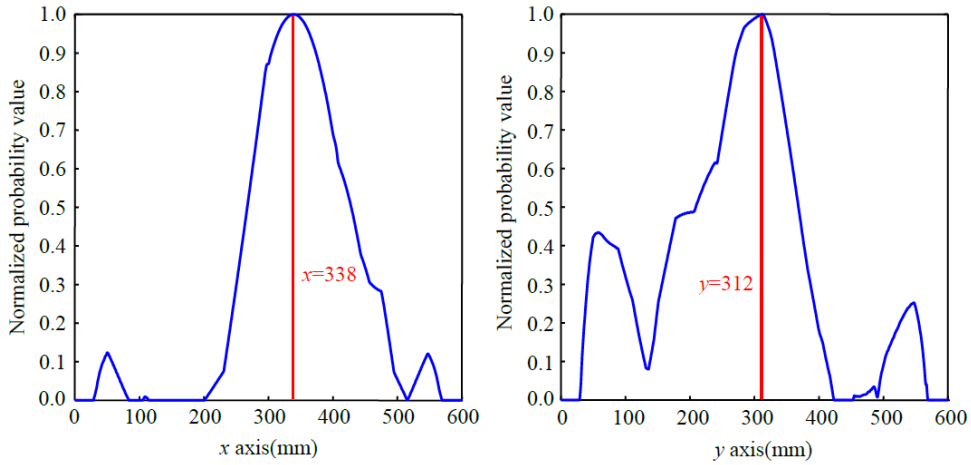

(a) Normalized probability value of *x* coordinates (b) Normalized probability value of *y* coordinates

Figure 11: Probability value curves after using modified method for the influence of UPDA.

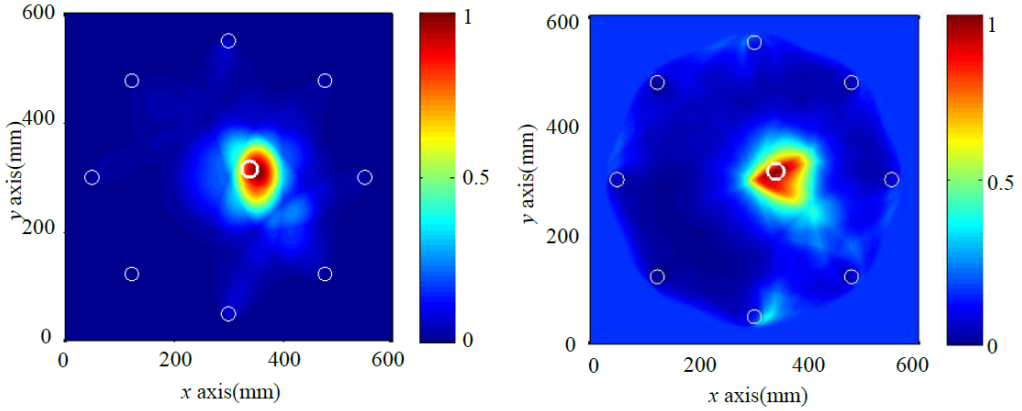

(a) Before using modified method (b) After using modified method

Figure 12: RAPID-based full multiplication imaging results before and after using modified method for the influence of UPDA.

3.5 Selection of imaging threshold based on ROC curve

Considering the influence of external disturbances such as input, environmental changes, low signal-to-noise ratio of EMAT, threshold is set in imaging to improve imaging accuracy. In RAPID, when the probability value of a point is greater than the threshold, it is identified that there exists damage at that point. We use ROC curve to determine the RAPID imaging threshold. Table 1 presents four events of damage identification may appear during the imaging process. The probability that E_1 and Y_1 occur at the same time is defined as the sensitivity which is denoted by S. The probability that E_2 and Y_2 occur at the same time is defined as the specificity. The probability of E_2 and Y_1 occur at the same time is defined as the false positive rate which is denoted by F. ROC curve is generated by describing the change between the sensitivity and the false positive rate at different thresholds [9, 10].

Events	Y_1: Damaged	Y_2: Undamaged
E_1: Detected	E_1 and Y_1 occur	E_1 and Y_2 occur
E_2: Undetected	E_2 and Y_1 occur	E_2 and Y_2 occur

Table 1: Four events of damage identification.

Figure 13 shows the ROC curve based on RAPID. Thresholds vary from 0 to 0.9 with an increment step of 0.1 and vary from 0.9 to 1.0 with an increment step of 0.01. The optimal threshold point is closest

to the (0, 1) point which the sensitivity is maximum and the false positive rate is minimum. In the Figure 13, the truncated curve is enlarged near the upper left corner, and when the threshold is 0.91, it is the closest to (0, 1). Figure 14 presents the threshold to take 0.91 to obtain RAPID imaging results. The imaging threshold greatly reduced the positioning range so that the location of simulated damage is obvious.

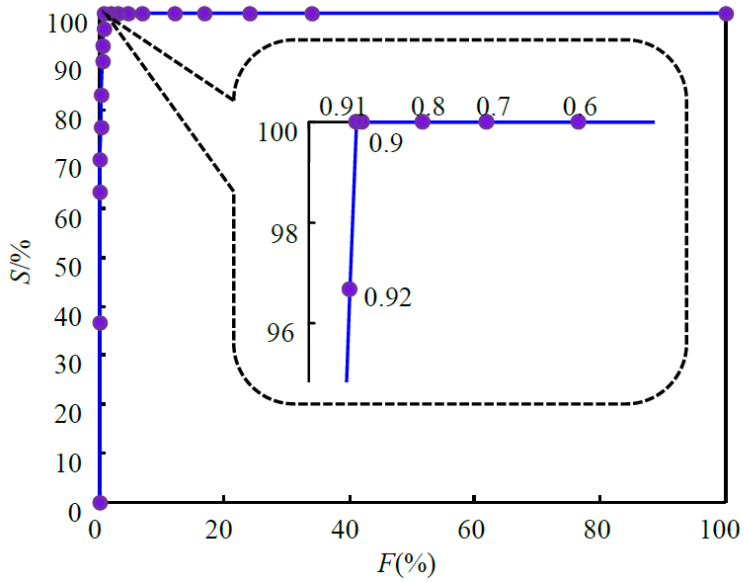

Figure 13: ROC curve based on RAPID.

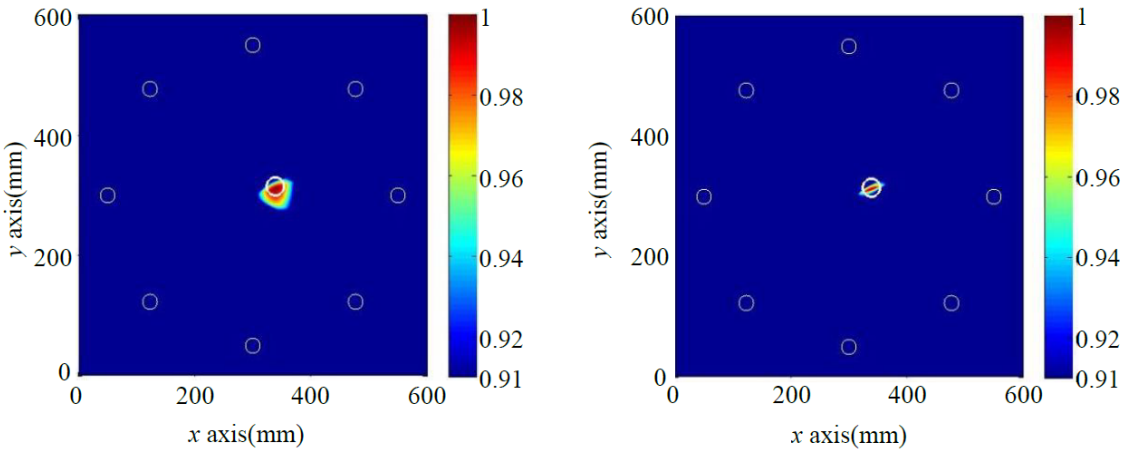

Figure 14: RAPID imaging results with threshold.

4 CONCLUSIONS

The method of SH waves combined with RAPID for damage imaging in composite plates is reported. SH_0 mode can be generated in the composite plate by double-turn coil OSH-MPT. Direct waves in baseline signals and damage signals are extracted to the same range to calculate A_{ij}. The β value of RAPID imaging coefficient is analyzed based on different sensing paths. Then, the appropriate β value which can be applied to eight circular transducer array of any diameter is chosen. The phenomenon of UPDA in RAPID is presented and modified methods are applied to eliminate the influence of UPDA on RAPID imaging. The feasibility of modified methods is verified in damage imaging experiments and the imaging accuracy is improved. The use of ROC curve to determine the RAPID imaging threshold is proposed. Imaging threshold greatly highlights damage position and improves the imaging contrast ratio.

By determining the reasonable β value, calculating A_{ij} value and eliminating the influence of UPDA, selecting imaging threshold, imaging detection can be achieved in composite plates through RAPID with MPT array.

ACKNOWLEDGEMENTS

This work was supported by the National Natural Science Foundation of China (Grant Nos. 51475012, 11527801, 11272021, and 51235001), the Scientific Research Project of Beijing Educational Committee (Grant No. KM201010005003), and the Importation and Development of High-Caliber Talents Project of Beijing Municipal Institutions (Grant No.CIT&TCD201304048).

REFERENCES

[1] P.J. Schubel, R.J. Crossley, E.K.G. Boateng and J.R. Hutchinson, Review of structural health and cure monitoring techniques for large wind turbine blades, *Renewable Energy,* **51**, 2013, pp. 113-123 (doi: 10.1016/j.renene.2012.08.072).

[2] Y.Y. Kim, Y.E. Kwon, Review of magnetostrictive patch transducers and applications in ultrasonic nondestructive testing of waveguides, *Ultrasonics,* **62**, 2015, pp. 3-19 (doi: 10.1016/j.ultras.2015.05.015).

[3] J.S. Lee, Y.Y. Kim and S.H. Cho, Beam-focused shear-horizontal wave generation in a plate by a circular magnetostrictive patch transducer employing a planar solenoid array, *Smart Materials and Structures,* **18**, 2009, pp. 1-9 (doi: 10.1088/0964-1726/18/1/015009).

[4] H.M. Seung, H.W. Kim and Y.Y. Kim, Development of an omni-directional shear-horizontal wave magnetostrictive patch transducer for plates, *Ultrasonics,* **53**, 2013, pp. 1304-1308 (doi: 10.1016/j.ultras.2013.03.015).

[5] T.R. Hay, R.L. Royer, H.D. Gao, X. Zhao and J.L. Rose, A comparison of embedded sensor Lamb wave ultrasonic tomography approaches for material loss detection, *Smart Materials and Structures,* **15**, 2006, pp. 946-951 (doi: 10.1088/0964-1726/15/4/007).

[6] X.L. Zhao, H.D. Gao, G.F. Zhang, B. Ayhan, F. Yan, C. Kwan and J.L. Rose, Active health monitoring of an aircraft wing with embedded piezoelectric sensor/actuator network: I. Defect detection, localization and growth monitoring, *Smart Materials and Structures,* **16**, 2007, pp. 1208-1217 (doi: 10.1088/0964-1726/16/4/032).

[7] Z.H. Liu, X.W. Zhong, T.C. Dong, C.F He and B. Wu, Delamination detection in composite plates by synthesizing time-reversed Lamb waves and a modified damage imaging algorithm based on RAPID, *Structural Control and Health Monitoring*, **24**, 2017, pp. e1919(17pp) (doi: 10.1002/stc.1919).

[8] Z.H. Liu, X.W. Zhong, M.W. Xie, X.C. Liu, C.F He and B. Wu, Damage imaging in composite plate by using double-turn coil omnidirectional shear-horizontal wave magnetostrictive patch transducer array, *Advanced Composite Materials,* **26**, 2017, pp. 67-78 (doi: 10.1080/09243046.2017.1313578).

[9] B. Park, H. Sohn, P. Malinowski and W. Ostachowicz, Delamination localization in wind turbine blades based on adaptive time-of-flight analysis of noncontact laser ultrasonic signals, *Nondestructive Testing and Evaluation,* **32**, 2017, pp. 1-20 (doi: 10.1080/10589759.2015.1130828).

[10] A.P. Bradley, The use of the area under the ROC curve in the evaluation of machine learning algorithms, *Pattern Recognition,* **30**, 1997, pp. 1145-1159 (doi: 10.1016/S0031-3203(96)00142-2).